

An edited version of this paper was published by AGU. Copyright 2006 American Geophysical Union: Jevrejeva, S., A. Grinsted, J. C. Moore, and S. Holgate (2006), Nonlinear trends and multiyear cycles in sea level records, *J. Geophys. Res.*, 111, C09012, doi:10.1029/2005JC003229.

Nonlinear trends and multi-year cycles in sea level records

S. Jevrejeva¹, A. Grinsted^{2,3}, J. C. Moore², and S. Holgate¹

1. Proudman Oceanographic Laboratory, Liverpool, UK
2. Arctic Centre, University of Lapland, Rovaniemi, Finland
3. Department of Geophysics, University of Oulu, Oulu, Finland

Abstract

We analyze the Permanent Service for Mean Sea Level (PSMSL) database of sea level time series using a method based on Monte Carlo Singular Spectrum Analysis (MC-SSA). We remove 2-30 year quasi-periodic oscillations and determine the nonlinear long-term trends for 12 large ocean regions. Our global sea level trend estimate of 2.4 ± 1.0 mm/yr for the period from 1993 to 2000 is comparable with the 2.6 ± 0.7 mm/yr sea level rise calculated from TOPEX/Poseidon altimeter measurements. However, we show that over the last 100 years the rate of 2.5 ± 1.0 mm/yr occurred between 1920 and 1945, is likely to be as large as the 1990s, and resulted in a mean sea level rise of 48 mm. We evaluate errors in sea level using two independent approaches, the robust bi-weight mean and variance, and a novel "virtual station" approach that utilizes geographic locations of stations. Results suggest that a region cannot be adequately represented by a simple mean curve with standard error, assuming all stations are independent, as multi-year cycles

within regions are very significant. Additionally, much of the between-region mismatch errors are due to multi-year cycles in the global sea level that limit the ability of simple means to capture sea level accurately. We demonstrate that variability in sea level records over periods 2-30 years has increased during the past 50 years in most ocean basins.

1. Introduction

The rate of global mean sea level rise over the last decade (1993-2000) determined from TOPEX/Poseidon altimeter measurements is 2.6 ± 0.7 mm/yr [White *et al.*, 2005], which is significantly larger than estimates (1-2 mm/yr) of the 20th century linear trend for sea level rise [Church *et al.*, 2001], and has reignited the discussion on whether sea level rise is accelerating. Long term sea level rates come from sea level gauge stations, that now number in excess of 1000. However, most of these stations were established in the 1950s, with only a handful extending back 100 years or more. According to White *et al.*, [2005] decadal trends in the global reconstruction of sea level vary from 0 to 4 mm/yr during the period 1950-2000, with a maximum during the 1970s. However, Holgate and Woodworth [2004] argue that in 10-year trends since 1950, the highest rates of sea level rise occurred in the 1990s, with the lowest rates in the 1980s.

In this paper we address the development of the regional and global nonlinear sea level trends over the full length of tide- gauge records, however as pre-20th century records are sparse and geographically very limited, we focus on the 20th century. We use several novel approaches in calculating mean sea level and errors for ocean regions and then analyze the sea level using Monte- Carlo Singular Spectrum Analysis (MC-SSA) with confidence intervals for nonlinear trends [Allen and Smith, 1996; Moore *et al.*, 2005]. This approach provides information on changes in contribution from 12 large ocean regions to global sea level rise over time. In addition, we use wavelet and wavelet

coherence methods [Torrence and Compo, 1998; Grinsted *et al.*, 2004] to investigate the role of signals with periods of 2-13.9 years in the variability of sea level records, their links to the large scale atmospheric circulation patterns and how these relationships have changed over the past 100 years.

In previously published results [see, e.g., Church *et al.*, 2001, Nerem and Mitchum, 2002], linear trends were calculated by ordinary least-squares methods, which can produce misleading results if the residuals do not have a white noise spectrum [Kuo *et al.*, 1990]. Additionally, most tide gauge records demonstrate distinctly non-uniform trends, which makes the linear trends sensitive to the arbitrarily chosen start and end dates. Here we apply MC-SSA to extract nonlinear long-term trends from time series of mean sea level. We filter the low frequency variability by removing the statistically significant 2-13.9 year oscillations associated with large scale atmospheric circulation [Unal and Ghil, 1995; Jevrejeva *et al.*, 2005]; along with multi-decadal oscillations (14-30 year periods). We then estimate the nonlinear long-term trend, providing the statistical significance of the trend, and its confidence intervals.

2. Data and Methodology

2.1. Tide gauge stations

We aimed to use all relative sea level (RSL) monthly mean time series in the Permanent Service for Mean Sea Level (PSMSL) database [Woodworth and Player, 2003]. However, data from Japan were excluded from the analysis due to uncertainty in earthquake-related land movement of bench marks and tide gauge stations. Detailed descriptions of the RSL time series are available from www.pol.ac.uk/psmsl. No inverted barometer correction was applied. RSL data sets were corrected for local datum changes and glacial isostatic adjustment (GIA) of the solid Earth [Peltier, 2001]. In the GIA data

set there were missing rates for several stations particularly in Arctic Siberia, and much of Australia. We addressed these deficiencies in GIA by assigning a station with no GIA correction the same GIA as the nearest station within 100 km of it. If no GIA corrected station was within 100 km, we used an interpolation scheme in assigning GIA rates from stations up to 1000 km away. Stations further than 1000 km from sites with assigned GIA were removed from the analyses.

There is no common reference level for the tide gauge records and this provides a problem when stacking records that do not cover the same time periods. One way overcome this problem is to calculate the rate of change in sea level for each station and stack the rates [Barnett, 1984]. However, many stations have historically only been measured for some months of the year and an annual cycle in sea level could therefore lead to severe bias. To maximize data usage, we calculate the mean annual rate for a given month over a whole year (e.g. the rate in January is calculated as the July to July difference). Using this method removes all systematic sub-annual signals from the data. Data gaps shorter than one year in the final rate series are filled by interpolation. This procedure results in data from 1023 stations containing 385324 individual monthly records, of which 22130 months were filled by interpolation. The maximum number of stations in any year is 585, with only 70 stations in 1900, and 5 in 1850. Due to the time lag between data collection and supply to the PSMSL recent decades have also seen reductions in station numbers with only 390 stations in 2000.

2.2 Regional trends

The geographical distribution of tide gauges provides a poor sampling of the ocean basins, and most of tide gauges are situated in the Northern Hemisphere (Europe, Japan and USA). Additionally tide gauge records do not cover the same time period. It is useful

to define 12 sea level regions (Figure 1) and calculate the mean sea level time series for the each region. The degree to which a station represents fluctuations in sea level across a region, and errors in the sea level measurements of stations are key issues in estimating region sea level trends. We use two independent methods of estimating these. The first is the standard method of the statistical bi-weight robust mean and variance [Mosteller and Tukey, 1977], commonly used in dendrochronology to produce mean indices that are robust in excluding time series that are far from the median series. This procedure leads to a mean and a standard error estimate directly from all the stations in a region. The second method we employ seeks to resolve the issue of spatial inhomogeneity. The stations are not evenly distributed spatially, and therefore we have developed a novel way of stacking the stations. Dealing separately with each region of the world ocean (Fig. 1), we recursively find the two closest stations (x and y) and merge them creating a new virtual station located half way between the original stations. The error for the virtual station for the i^{th} year can be written as

$$e_i = \sqrt{m_i^2 + r_i^2}, \quad (1)$$

where m is the measurement error associated with each station measurement and r is the misfit error, that is the difference in sea level trend recorded at the two stations in any particular year. The error e is treated as a measurement error when a virtual station is merged with another station in the next step in the recursion. Generally time series from x and y do not span exactly the same period. The mean measurement error (m) is then calculated as

$$m_i = \frac{\sqrt{m_{x,i}^2 + m_{y,i}^2}}{n_i}, \quad (2)$$

where m_x and m_y are the measurement errors of station x and y respectively. In years where only one station has data $n_i = 1$ and the other is simply left out of the equation,

otherwise $n_i=2$. The misfit error tells how well the virtual station represents stations x and y and is written

$$r_i = \frac{\sigma_{xy}}{2\sqrt{n_i}}, \quad (3)$$

where σ_{xy} is calculated as the standard deviation of the rates at x minus those at y over the interval of common overlap. When the recursive procedure has been carried out we are left with the sea level rate of the entire region and its associated error.

Figure 2 shows the yearly sea level rate of change in the eastern North Atlantic region with the bi-weight mean and the virtual station method. The general features agree well over most of the full length of the record, though it can be seen that the bi-weight mean estimate tends to have smaller amplitude in some periods where statistical outliers are removed from the robust mean. Note that there is very little overall trend apparent in the rate curve. The variation in the standard errors shows more interesting differences between the methods. In the early part of the record, when there are few stations, the two methods give quite similar estimates of the errors. However when the number of stations becomes much larger in the middle of the 20th century, the bi-weight standard error becomes much smaller than the virtual station estimate. This is because the simple assumption of statistical independence inherent in the bi-weight method, reduces the standard error of the mean by the square root of the number of stations. However the virtual station error remains large as it is dominated by the station mismatch error in the final step of the recursion process, when two far-apart stations that generally have large mismatch, are meaned. This reflects the true limit of how representative a single curve is of region-wide sea level. Therefore the virtual station error is a much more reliable estimate of uncertainty than a simple robust standard error.

2.3 Global sea level

Previous authors have used estimates of the linear trends for oceanic basins (found by averaging the basin rates) to compute a simple global trend by taking the mean and the error in the mean between basins [Douglas, 1997]. Simple averaging of these errors would lead to incorrect uncertainties in sea level rise. Despite the relatively large virtual station error estimates, we find that integrating the trends results in positive rates in all regions over the last 150 years. This strongly suggests that errors in rates are not random, but caused by systematic oscillations in sea level within the regions which will be manifested as autocorrelation within the errors. We define a region mismatch error (b_i) as the difference in sea level rates between that in the particular region and the mean over all the regions in the i^{th} year. We can correct for the autocorrelated fraction of the b_i error by considering its power spectrum (Figure 3). The power spectrum shows a marked decrease with frequency, due to the importance of multi-year oscillations in sea level. Since the low frequencies dominate the total mismatch error, we should reduce the mismatch error estimate on the yearly rates by the square root ratio of the high frequency power to the low frequency power, (P). From Figure 3 it can be seen that this ratio is typically about 2-3 and so the between-region sea level yearly rate error estimate should be only about 1/2 of the standard error found simply by considering the rates between regions. To calculate the total error in the global trend (g_i) we need to add (as a vector) this between-region error to the station representativity error (again correcting for the power spectrum of the error).

$$g_i = P \sqrt{b_i^2 + \frac{\sum_j e_{ij}^2}{N_i^2}} \quad (4)$$

where N_i is the number of regions with stations operating in the i^{th} year, and e_{ij} is the e_i from Equation (1) in j^{th} region. This is the error that we shall report in global rate estimates.

2.4 Sea level analysis

In this study the sea level time series were considered as a combination of the long-term trends, oscillations and noise. For trend analysis we use a novel approach [Moore *et al.*, 2005] that has significant advantages over traditional low pass filtering in that we can estimate the significance of the trend, its confidence intervals and its contribution to the total series variance. We decompose the time series using the MC-SSA [Allen and Smith, 1996] with data-adaptive orthogonal filters, separating the original time series into the nonlinear low frequency trend, quasi-periodic signals and noise, distributed among the filters. We use an embedding dimension of equivalent to 30 years, which means low frequency oscillations will appear as trends in a similar way to filtering with a Gaussian of 60 year cut-off period [Moore *et al.*, 2005]. We calculate the statistical significance of components reconstructed by convoluting the original series with each of the filters and comparing against red noise models (Monte Carlo method, with 1000 surrogate series with the same length, observed variance and lag-one autocorrelations as the original time series). All results presented in this paper are statistically significant at the 95% level against white noise models, and many are also significant against red noise models. The contribution from the trends and quasi-regular oscillations to the total variance, are calculated as a projected component relative to the original time series. Finally, we remove the effects of the short time scale variability (2-30years) from the time series, then extract the long-term trends and analyze their development over time. Mann [2004] discusses methods of calculating trends close to the observational boundaries, and we use

a variation on the minimum roughness criterion here. We implement the minimum roughness by extrapolate the time series 30 years forward and backward in time using a least squares linear fit of to the 30 years of data nearest to a boundary before applying the SSA non-linear trend filter. The nonlinear trend at the data boundaries may therefore be said to be composed of 30 data points and 29 extrapolated points from the linear trend.

In comparison with the least squares linear fits, often used to compute confidence intervals of means, we have the advantage of requiring errors to conform only to the optimal data adaptive filter specifying the trend, and thus find that confidence intervals in nonlinear time series are perhaps 3-4 times smaller than found by linear fitting [*Moore et al.*, 2005].

Nonlinear trends for regional sea level yearly rate are calculated from the integrated mean regional monthly rates to give a sea level curve, then performing MC-SSA to extract the nonlinear trend and finally differentiating to give the nonlinear trend in regional sea level rate. This method avoids uncertainties in decomposing the monthly rate where the trend accounts for a small fraction of the variance in the data, whereas using the integrated data the trend often accounts for 50% of the variance.

Global sea level rate is calculated by simply averaging the regional rates (the Baltic being excluded, as discussed later). Global sea level is found from the mean of the regional sea level curves. The error in global sea level is estimated from the standard deviation of the regional sea level curves for each year, however, the errors produced are not statistically independent for similar reasons as those discussed earlier in relation to equation (4), and so we estimate the confidence interval using a “jack knife” method [*Press et al.*, 1992] which can compensate for this effect.

To investigate the role of 2-30 year oscillations we use MC-SSA and wavelet methods. We apply the wavelet method [*Torrenco and Compo*, 1998] and decompose the

time series into time –frequency space, in order to determine both the dominant modes of variability and how those modes vary in time. We compare results with the oscillations detected by MC-SSA, and the consistency of the results obtained by these independent methods strengthens their credibility.

To analyze the direct links between the statistically significant components in regional sea level time series and time series representing the large scale atmospheric circulation we use the wavelet coherence method [*Grinsted et al.*, 2004; *Jevrejeva et al.*, 2005]. We give descriptions of the changes in covariance between time series and show that there is considerable linkage between the statistically significant components in time series of sea level and atmospheric circulation.

3. Results

3.1 Nonlinear trends in sea level

Figure 4 shows the rates of the nonlinear trends in 10 of the 12 regions (Antarctic and Southeastern Pacific, time series are too short to perform trend analysis). Figure 5 shows the mean global sea level and its non-linear trend with 95% confidence interval, and also the nonlinear global sea level rate. Only 5 stations were active during 1850 and all of them were in the North Atlantic or the Baltic (Figure 4), so estimates of global trends are rather uncertain before 1900, as is reflected in the large errors in Figure 5. The large acceleration in sea level 1850-1870 coincides with a few new stations becoming active, and is probably not statistically significant.

In contrast with linear trends, where the rate of mean sea level rise is constant, our results (Figure 4) reveal the evolution of sea level rise during the 20th century and show that the highest regional rates of up to 3-5 mm/yr occurred between 1920-1950 (with some regional variations, e.g. the later maximum for the Southwestern Atlantic and

Western Pacific). The major contributions to the global sea level rise during 1920- 1940 are from the Northwestern Atlantic (4.2 ± 1.0 mm/yr), Indian (3.5 ± 1.0 mm/yr), and Mediterranean (3.1 ± 1.0 mm/yr) regions. Even smoothed by the 30 year SSA window, the trends from the different ocean regions show slightly dissimilar patterns and still demonstrate some cyclic variability. This cyclicity is associated with longer term oceanic variations [e.g. *Ghil*, 2001], changes in thermal expansion and water mass adding to the ocean, which may provide non uniform regional sea level rise, and melting of continental ice leads to the significant geographic variations in the sea level change due to both gravitational and loading effects [*Mitrovica et al.*, 2001].

A notable feature of Figure 4 is that for the last 20 years the regional trends are more coherent in the sense that the trends are closely grouped, and the rates for the southern and northern hemisphere become similar. The trend for the Baltic Sea is strongly influenced by limited water exchange with larger regions and fresh water flux variations [*Meier and Kauker*, 2003] which leads to its rate curve being quite dissimilar from the other regions, and in our study we have excluded the Baltic Sea time series from the calculation of the global sea level trend. Arctic sea level trend has been accelerating for the last 30 years, which can be explained by the warming of the Arctic coupled with increased influx of warmer Atlantic waters to the arctic region, the increase of fresh water inflow from Siberian rivers [*Dickson et al.*, 2002, *Wu et al.*, 2005], and changes in the Arctic Ocean circulation [*Proshutinsky et al.*, 2001].

Applying a least squares linear regression analysis to the global sea level in Figure 5 gives a trend of 1.8 mm/yr between 1900 and 2000, as found in earlier studies [*Church et al.*, 2001]. However, our results show that global sea level rise is irregular and varies greatly over time, it is apparent that rates in the 1920-1945 period are likely to be as large as today's. Nevertheless, considerable uncertainties remain.

The nonlinear trend for the 1990s show about the same sea level rise (2.4 ± 1.0 mm/yr) as TOPEX/Poseidon, which demonstrates the ability of the nonlinear trend to resolve (with certain errors) the temporal evolution of the spatial sea level field. The largest contributions to the global sea level trend during the 1990s are from Northwestern Atlantic, Northeastern Atlantic and Arctic regions (Figure 4), which is in good agreement with results from *Levitus et al.* [2005] showing the warming of the Atlantic regions providing the largest contribution to the global ocean heat content during 1955-2003.

Sea level is an integrated indicator of climate variability, which reflects changes in the dynamic and thermodynamic in atmosphere, ocean and cryosphere. Both land surface [*Jones and Moberg, 2003*] and sea surface temperature data [*Kaplan et al., 1998, Rayner et al., 2003*] are in good agreement with the gsl curve in Figure 5. In particular, the increases from 1910 to 1940, and from 1980 until the present, as well as a stagnation between 1940-75. One possible explanation for the sea level acceleration during 1920-1945 was the low level of volcanic activity. Recently published model results [*Church et al., 2005*] suggests that multi-year to decadal sea level variability is significantly affected by volcanic activity. The climate system responds to volcanic forcing on a range of time scales. The short period (generally lasting 1-3 yrs) response is mainly due to stratospheric aerosols from explosive volcanic eruptions scattering incoming solar short wave radiation, which leads to cooling of the global average temperature [*Sato et al., 1993, Robock and Liu, 1994; Robock, 2000*] and a reduction in rainfall [*Robock and Liu, 1994, Gillet, et al., 2004, Lambert et al., 2004*]. A simple comparison between the rate of sea level rise and stratospheric aerosol optical thickness, the principal parameter affecting stratospheric aerosol climate forcing [*Sato et al., 1993*], is shown in Figure 6 and suggests that rapid sea level rise prior to 1980 occurred during periods of low volcanic activity. While it is tempting to perform regression modeling of sea level on the trends in optical depth and

e.g. global temperature, it is problematic as the short term volcanic impact on global temperatures means that the variables are highly co-dependent. Applying regression on MC-SSA trend data (effectively moving averaged with a 60 year window) reduces the available degrees of freedom in 150 years of data to the point where fits are statistically insignificant. However, our hypothesis is supported by the results from the SI200 version of Goddard Institute for Space Studies (GISS) simulations, where since 1950, minima in the ocean heat content occurred due to the large volcanic eruptions of Agung, El Chichon and Pinatubo [*Hansen et al.*, 2002]. The observed ocean heat content [*Levitus et al.*, 2005] provides evidence of cooling after all three eruptions (Agung, El Chichon and Pinatubo). *Bengtsson et al.* [1999] also demonstrate that the Pinatubo eruption had a recognizable effect on climate, with direct forcing limited in duration to a few years and a long-term effect, lasting 7 years, due to cooling of the oceans.

3.2 The role of oscillations in the 2-30 year band

Using MC-SSA we extract statistically significant components from time series of regional sea level. Signals in the 3.5-13.9 year band contribute from 5 to 20 % of variability in time series. There is also a substantial contribution from signals with 13-30 year periodicity. In our study signals with 13-30 year periodicity from regional time series are statistically significant against a white noise model. However, for individual stations these signals are statistically significant against red noise [*Unal and Ghil*, 1995]. Our results are in good agreement with oscillations detected at 3.5, 5.2- 5.7, 7-8.5 and 10-13.9 years for individual sea level station time series by *Unal and Ghil* [1995]. It is notable that 3.5-13.9 year oscillations demonstrate an increase in amplitude since the 1940s in several regions – Northeastern Atlantic, Northwestern Atlantic, Eastern Pacific, presented in Figure 7.

To isolate the different timescales of variability, and analyze the changes of variance in the time series of sea level we examine their behaviour in time-frequency space using the Morlet wavelet. Figure 8 shows the wavelet power spectrum of 4 regional sea level time series, displayed as a function of cycle period and time. The left axis is the Fourier period; the bottom axis shows the time in years. The strong non-stationary behaviour of the spectra is clearly seen. Most of the time series show an increase of power in the wavelet power spectrum at 2-30 year periods since 1940s.

Oscillations in the 2.2-7.8 year band in individual sea level records have been associated with large scale atmospheric circulation signals [*Unal and Ghil, 1995; Jevrejeva et al., 2005*], which generate a sea level response through a number of processes: the direct influence of changed atmospheric pressure, changes in wind stresses, and changes in atmosphere- ocean fluxes as well as storm surges. Previously published results have revealed the influence of large scale atmospheric circulation on sea level variability for various ocean basins. According to the *Hughes et al. [2003]* Antarctic sea level is highly coherent with the Antarctic Annular Mode (AAO). Substantial contributions from changes in large scale atmospheric circulation patterns to the sea level variability in Arctic was found by *Proshutinsky et al. [2001]*. The role of the SOI index in variability in the Pacific sea level is discussed by *Church et al. [2004]*.

To identify the frequency bands within which time series of sea level and the large scale atmospheric circulation are co-varying, we use the wavelet coherency method [*Grinsted et al., 2004; Jevrejeva et al., 2005*]. Figure 9a demonstrates the influence of the Arctic Oscillation (AO) [*Thompson and Wallace, 1998*] on the variability of the North Atlantic associated with 2.2-13.9 year signals after 1940, which is in excellent agreement with results for the individual records reported by *Jevrejeva et al. [2005]*. Influence of the North Atlantic Oscillation (NAO) [*Jones et al., 1997*] in the Mediterranean region, shown

by *Tsimplis and Josey* [2001], is associated with 2.2-7.8 year signals (Figure 9b). There is also evidence of a shift in the period of maximum coherence from the 2.2- 3.5 to the 3.5-7.8 year band for the Northeastern Atlantic after 1950 and noticeable changes in the 2.2-5.7 year band for the Mediterranean region.

Indian and Pacific oceans sea level variability is mainly associated with Southern Oscillation Index (SOI) [*Ropelewski and Jones*, 1987] signals at 2.2, 3.5, 5.7 year periods. Figures 9c,d demonstrate that the relationship is not stationary and the influence of SOI has generally increased over the last 60 years over a broadening spectrum of periods. Our results (Figure 9d) show increasing influence from 13.9 year signal, previously found in Sea Surface Temperature (SST) in the Pacific Ocean and extending to the polar regions [*Jevrejeva et al.*, 2004]. We also use the Pacific Decadal Oscillation (PDO) index [*Zhang et al.*, 1997], derived as the leading mode of monthly SST anomalies in the North Pacific Ocean, as a representation of the Pacific climate variability. The signature of the 2.2-30 year signals, associated with PDO, is clearly seen in the Eastern Pacific sea level variability (not shown here). The PDO's influence since 1940, shows an increase in the low frequency power in the 13-30 year band, somewhat similar to seen for the SOI in Fig. 9d, and large changes in the 3.5-7.8 year band. Our results are consistent with a previous study by *Church et al.* [2004] where SOI was found to be strongly anti-correlated (-0.78) with the first Empirical Orthogonal Function (EOF) of sea level in the Pacific. Furthermore, increased variance in sea level is associated with a tendency for ENSO events to be more frequent, persistent and intense in the equatorial Pacific in the last two decades.

4. Discussion

Our global sea level trend estimate of 2.4 ± 1.0 mm/yr for the period from 1993 to 2000 matches the 2.6 ± 0.7 mm/yr sea level rise found from TOPEX/Poseidon altimeter data. However, Figure 5 suggests that during 20th century a similar sea level rise was observed between 1920 and 1945. The maximum rate of global mean sea level rise was 2.5 ± 1.0 mm/yr during the period 1920-45, with cumulative rise of 48 mm in 25 years.

These results differ slightly from previously published conclusions [e.g. *Cazenave and Nerem, 2002*] concerning historical rates of mean sea level rise during recent decades. Most probably the difference in the results can be explained by the use of different data (number of stations, location of the stations), GIA corrections, methods and errors for trend calculation. *Church et al. [2004]* pointed out that with decadal variability in the computed global mean sea level, it is not possible to detect a significant increase in the rate of sea level rise over the period 1950-2000. However, results from *White et al. [2005]* suggest that decadal reconstructed sea level trends have varied from 0 to 4 mm/yr since 1950. The results of *Holgate and Woodworth [2004]* for the second half of the 20th century reveal that the highest rates in decadal sea level trends were in the 1990s, but the lowest rises were in the 1980s, demonstrating a significant variation in rates of sea level rise.

Furthermore, observed ocean heat content, the major contributor to sea level rise, has significant decadal variability [*Levitus et al., 2005*]. According to results from simulations using the GISS global climate model these decadal heat content changes do not appear to be caused by the climate forcing, but are more likely to be dynamical features [*Hansen et al., 2002*]. Similar results are found with the National Centre for Atmospheric Research (NCAR) Parallel Climate Model [*Barnett et al., 2001*]. Multi-decadal variability in sea level records most probably links to the variability in the heat

transported by the thermohaline circulation, driven by the temperature and salinity differences [Deser and Blackmon, 1993; Rajagopalan et al., 1998; Rodwell, et al., 1999]. Such changes in the thermal structure of the ocean can result in steric (density) sea level changes [Knutti and Stocker, 2000].

Our results show that there is an increase in 2-30 year variability in sea level over the recent decades for several regions. We speculate that one of the possible sources for increase in 2-13.9 year variability could be the large scale atmospheric circulation represented by the SOI, AO, NAO and PDO.

Figure 4 shows some evidence that the nonlinear trends for the different regions are in closer agreement around 1980 than previously, though it must be noted that errors in the trends are relatively large. Additionally Figure 8 shows that 2-30 year variability is increasing. One possible explanation is a warmer ocean makes the large scales more coherent, as ocean temperature and heat content increase in all regions of the world. At the same time, the 2-13.9 year variability in sea level records in some regions, for example North Atlantic, Mediterranean sea, Eastern Pacific, Indian oceans associated with atmospheric forcing, which has increased over the last 50 years [Wakelin et al., 2003; Jevrejeva et al., 2005], shows the relationship is changing with time. This phenomenon may be expected on theoretical grounds [e.g. Tsonis, 2004]. It is likely as a warmer ocean leads to more large scale teleconnections, while also tending to introduce more variability at any particular place [Tsonis, 2004]. This can be seen in Fig. 9d where long period signals increase in strength and generally the Pacific sea level at all frequencies is seen to be more coherent with SOI. Increases in high frequency coherency in the Pacific (Fig. 9d) are also suggestive of the increasing frequency of El-Nino events [Church et al., 2004]. Similar results are seen in many other records of the climate system, for example global temperature records [Jones and Moberg, 2003] and 500 mbar pressure

height fields [Tsonis, 2004]. The manifestation of the climatic mechanisms responsible for the increased long-range teleconnections is presently little understood, but must be related to the low-order dynamics of the global system, for example the increasing rate of El-Nino events, and reduction in La Nina in a warming world discussed by Tsonis *et al.* [2005].

Our study shows the importance of estimates of uncertainties and hence some of the limitation of tide gauges measurements, previously pointed out by Church *et al.* [2004], Cazenave and Nerem [2004]. In our method the estimates explicitly account for the spatial redistribution of sea level, and record the temporal variability better than estimations from individual stations. The errors in the estimates are inevitably quite large, due to the poor special distribution of tide gauges, as they are located only on the continental margins and ocean islands. The alternative method of producing a mean sea level curve by choosing tide gauges from suitable locations by selective criteria, as used by Douglas [1997], reduces the number of useful tide gauges to very few (25). Thus a producing possibly larger error source for sea level estimates [Cazenave and Nerem, 2004]. Our results show that error can be reduced with substantial increase of number of tide gauge records; for example, for the period 1800-1900 the errors are 2-3 mm/yr, compare to 1 mm/yr during 20th century.

Conclusion

We developed a new “virtual station” method of analyzing sea level records from across different oceanic regions. This is statistically more appropriate than assuming independent errors from all stations in a region, as there are important multi-year cycles in sea level that have different phase lags at stations across an ocean region. We can then get an appropriate sea level curve for each region, and importantly, an error estimate is also

produced that can then be used in analysis of the non-linear trend from SSA with confidence intervals.

We have shown that the development of global sea level rise is highly dependent on the time period chosen and the global sea level rise occurred during the period from 1920 to 1945 is comparable with present day rate of sea level rise. Nonlinear sea level trends for the ocean regions are non uniform even after 30 year smoothing (trends in high latitude ocean regions have huge uncertainties, which is a challenge for future study). We provide evidence that 2-13.9 year variability in sea level records is increasing during the past 50 years for most of the ocean basins.

Our study demonstrates the importance of identifying the effect of multi-year to decadal scale anomalies on sea level trends in very short time series. We also show that low –frequency, multi-decadal variability is significant and that linear trends do not properly represent this. By removing the high frequency variability we reduce the uncertainties associated with redistribution of sea level due to varying geographical locations of tide gauges along the coastline as well as noise associated with coastal processes and determine the sea level rise driven by the climatic forcing.

We demonstrate that advanced statistical methods improve error estimations and reduce uncertainties for calculation of regional and global sea level rise. However, the main source for the uncertainties in sea level studies using tide gauge records still remain: poor historical distribution of tide gauges, lack of the data from Southern hemisphere (Africa and Antarctica), the GIA corrections used, and localized tectonic activity.

Acknowledgements

Some of our software includes code originally written by E. Breitenberger of the University of Alaska adapted from the freeware SSA-MTM Toolkit: <http://www.atmos.ucla.edu/tcd/ssa>. We thank the Thule Institute and Finnish Academy for financial support, two anonymous referees provided useful comments.

References

- Allen, M.R., and L.A. Smith (1996), Monte Carlo SSA, detecting irregular oscillations in the presence of coloured noise, *J. Clim.*, 9, 3383-3404.
- Barnett, T. P. (1984), The estimation of "global" sea level change: a problem of uniqueness, *J. Geophys. Res.*, 89(C5), 7980-7988.
- Barnett, T.P., D.W. Pierce and R. Schnur (2001), Detection of antropogenic climate change in the world's oceans, *Science*, 292, 270-274.
- Bengtsson, L., E. Roeckner, and M. Stendel (1999), Why is the global warming proceeding much slower than expected?, *J. Geophys. Res.*, 104, 3865-3876, 10.1029/1998JD200046.
- Cazenave, A., and R.S. Nerem (2002), Geophysics: Redistributing Earth's mass, *Science*, 294, 840-842.
- Cazenave, A., and R.S. Nerem (2004), Present-day sea level change: observations and causes. *Rev. Geophys.*, 42, 2003RG000139.
- Church, J.A., J.M. Gregory, P. Huybrechts, M. Kuhn, K. Lambeck, M.T. Nhuan, D. Qin, and P.L. Woodworth (2001), Changes in Sea Level. In *Climate Change 2001: The Scientific Basis. Contribution of Working Group 1 to the Third Assessment Report of the Intergovernmental Panel on Climate Change*. Houghton, J.T., Y. Ding, D.J. Griggs, M. Noguer, P. van der Linden, X. Dai, K. Maskell and C.I. Johnson, eds, Cambridge University Press, 639-694.

Church, J.A., N.J. White, R. Coleman, K. Lambert, and J.X. Mitrovica (2004), Estimates of the regional distribution of sea level rise over the 1950-2000 period, *J. Clim.*, 17, 2609-2625.

Church, J.A., N.J. White, and J.M. Arblaster (2005), Significant decadal-scale impact of volcanic eruptions on sea level and ocean heat content, *Nature*, 438, 74-77.

Deser, C., and H.-G. Blackmon (1993), Surface climate variations over the North Atlantic Ocean during winter: 1900-1989, *J.Clim.*, 6, 1743-53.

Dickson, B., I. Yashayaev, J. Meincke, B. Turrell, S. Dye and J. Holfort (2002), Rapid freshening of the deep North Atlantic Ocean over the past four decades, *Nature*, vol 416, 832 – 837.

Douglas, B.C. (1997), Global Sea Rise: A Redetermination. *Surveys in Geophysics*, 18, 270-292.

Ghil, M. (2001), Natural climate variability, in *Encyclopedia of Global Environmental Change*, T. Munn (Ed.), Vol. 1 (M. MacCracken and J. Perry, Eds.), J. Wiley & Sons, Chichester/New York, pp. 544–549.

Gillett N. P., A. J. Weaver, F. W. Zwiers, and M. F. Wehner (2004), Detection of volcanic influence on global precipitation, *Geophys. Res. Lett.*, 31, 10.1029/2004GL020044.

Grinsted, A., J.C., Moore, and S. Jevrejeva (2004), Application of the cross wavelet transform and wavelet coherence to geophysical time series, *Nonlinear Processes in Geophysics*, vol 11, 5/6, 561-566.

Hansen, J., Mki. Sato, L. Nazarenko, R. Ruedy, A. Lacis, D. Koch, I. Tegen, T. Hall, D. Shindell, B. Santer, P. Stone, T. Novakov, L. Thomason, R. Wang, Y. Wang, D. Jacob, S. Hollandsworth, L. Bishop, J. Logan, A. Thompson, R. Stolarski, J. Lean, R. Willson, S. Levitus, J. Antonov, N. Rayner, D. Parker, and J. Christy (2002), Climate forcings in

Goddard Institute for Space Studies SI2000 simulations, *J. Geophys. Res.*, 107, no. D18, 4347, doi:10.1029/2001JD001143.

Holgate, S. J., and P.L. Woodworth (2004), Evidence for enhanced coastal sea level rise during the 1990s, *Geophys. Res. Lett.*, 31, 2004GL019626.

Hughes C. W., P. L. Woodworth, M. P. Meredith, V. Stepanov, T. Whitworth, and A. R. Pyne (2003), Coherence of Antarctic sea levels, Southern Hemisphere Annular Mode, and flow through Drake Passage, *Geophys. Res. Lett.*, 30 (9), 1464, 2003GL017240.

Jevrejeva, S., J. C. Moore, and A. Grinsted (2004), Oceanic and atmospheric transport of multi-year ENSO signatures to the polar regions, *Geophys. Res. Lett.*, Vol. 31, No. 24, 10.1029/2004GL020871.

Jevrejeva, S., J. C. Moore, P. L. Woodworth and A. Grinsted (2005), Influence of large scale atmospheric circulation on the European sea level: results based on the wavelet transform method, *Tellus A*, 57A, 129-149.

Jones, P.D., T. Jonsson, and D. Wheeler (1997), Extension using early instrumental pressure observations from Gibraltar and SW Iceland to the North Atlantic Oscillation, *Int. J. Climatol.* 17, 1433-1450.

Jones, P.D. and A. Moberg (2003), Hemispheric and large-scale surface air temperature variations: An extensive revision and an update to 2001, *J. Clim.*, 16, 206-223.

Kaplan, A., M. A. Cane, Y. Kushnir, A.C. Clement, M.B. Blumenthal, and B. Rajagopalan (1998), Analyses of global sea surface temperature 1856-1991, *J. Geophys. Res.*, 103, 18567-18589.

Knutti, R., and T.F. Stocker (2000), Influence of the thermohaline circulation on projected sea level rise, *J. Clim.*, 13, 1997-2001.

Kuo, C., Lindberg, C., and D.J. Thomson (1990), Coherence established between atmospheric carbon dioxide and global temperature, *Nature*, 343, 709- 713.

Lambert F. H., P. A. Stott, M. R. Allen, and M.A. Palmer. 2004. Detection and attribution of changes in 20th century land precipitation, *Geophys. Res. Lett.*, 31, doi:10.1029/2004GL019545.

Levitus, S., J.I. Antonov, and T.P. Boyer (2005), Warming of the world ocean, 1955-2003, *Geophys. Res. Lett.*, Vol. 32, 2004GL021592.

Mann, M. (2004), On smoothing potentially non-stationary climate time series, *Geophys. Res. Lett.*, 31, 2004GL019569.

Meier, H.E.M, and F. Kauker (2003), Modeling decadal variability of the Baltic Sea: 2. Role of freshwater inflow and large-scale atmospheric circulation for salinity. *J. Geophys. Res.* 108, 3368, 10.1029/2003JC001799.

Mitrovica, J.X., M.Tamisiea, J.L. Davis, and G.A. Milne (2001), Recent mass balance of polar ice sheets inferred from patterns of global sea-level change. *Nature*, 409, 1026-29.

Moore, J.C., A. Grinsted and S. Jevrejeva (2005), The new tools for analyzing the time series relationships and trends. *EOS*, vol., 86, 24.

Mosteller, F. and J. Tukey (1977), *Data Analysis and Regression*, Addison-Wesley.

Nerem, R.S., and G.T. Mitchum (2002), Estimates of vertical crustal motion derived from differences of TOPEX/Poseidon and tide gauge sea level measurements, *Geophys. Res. Lett.* 29, 10.1029/2002GL015037.

Peltier, W.R., (2001), Global glacial isostatic adjustment and modern instrumental records of relative sea level history. In *Sea Level Rise*, Douglas, B.C., Kearney, M.S.,and S.P. Leatherman (Eds.), Academic Press.

Press, W.H., Flannery, B., Teukolsky, S.A., and W. Vetterling (1992), *Numerical Recipes in C*, 2nd ed., Cambridge University Press.

Proshutinsky, A., V. Pavlov, and R. H. Bourke (2001), Sea level rise in the Arctic Ocean, *Geophys. Res. Lett.*, 28(11), 2237-2240, 10.1029/2000GL012760.

Rajagopalan, B., Kushnir, Y., and Y.M. Tourre (1998), Observed decadal midlatitude and tropical Atlantic climate variability, *Geophys. Res. Lett.*, 25, 3967-3970.

Rayner, N. A., D.E. Parker, E.B. Horton, C.K. Folland, L.V. Alexander, D.P. Rowell, E.C. Kent, and A. Kaplan (2003), Global analysis of sea surface temperature, sea ice, and night marine air temperature since the late nineteenth century, *J. Geophys. Res.*, 108, D14, 10.1029/2002JD002670.

Robock, A., and Y. Liu (1994), The Volcanic Signal in Goddard Institute for Space Studies Three-Dimensional Model Simulations, *J. Clim.*, 7, 44-55.

Robock, A. (2000), Volcanic Eruptions and Climate, *Rev. Geophys.*, 38 (2), 191-220, doi:10.1029/1998RG000054.

Rodwell, M.J., Rowell, D.P., and C.K. Folland (1999), Oceanic forcing of the wintertime North Atlantic Oscillation and European climate, *Nature*, 398, 320- 323.

Ropelewski, C.F., and P.D. Jones (1987), An extension of the Tahiti-Darwin Southern Oscillation Index, *Monthly Weather Review*, 115, 2161-2165.

Sato, M., J.E. Hansen, M.P. McCormick, and J.B. Pollack (1993), Stratospheric aerosol optical depth, 1850-1990, *J. Geophys. Res.*, 98, 22987-22994.

Thompson, D.W.J., and J.M. Wallace (1998), The Arctic Oscillation signature in the winter geopotential height and temperature fields, *Geophys. Res. Lett.*, 25, 1297-1300.

Torrence, C., and G.P. Compo (1998), A practical guide to wavelet analysis. *Bull. Am. Meteorol. Soc.* 79, 61-78.

Tsimplis, M.N., and S.A. Josey (2001), Forcing of the Mediterranean Sea by atmospheric oscillations over the North Atlantic. *Geophys. Res. Lett.*, 28, 803-806.

Tsonis, A.A. (2004), Is Global Warming Injecting Randomness Into the Climate System? *EOS*, vol., 85, 38.

Tsonis, A.A., J.B. Elsner, A.G. Hunt, and T.H. Jagger (2005), Unfolding the relation between global temperature and ENSO, *Geophys. Res. Lett.*, 32, 10.1029/2005GL022875.

Unal, Y.S., and M. Ghil (1995), Interannual and interdecadal oscillation patterns in sea level, *Clim. Dyn.*, 11, 255-278.

Wakelin, S. L., Woodworth, P.L., Flather, R. and J.A. Williams (2003), Sea-level dependence on the NAO over the NW European Continental Shelf, *Geophys. Res. Lett.*, 30, 10.1029/2003GL017041.

White N. J., J. A. Church, and J. M. Gregory (2005), Coastal and global averaged sea level rise for 1950 to 2000, *Geophys. Res. Lett.*, 32, doi:10.1029/2004GL021391.

Woodworth, P.L., and R. Player (2003), The Permanent Service for Mean Sea Level: an update to the 21st century, *Journal of Coastal Research*, 19, 287-295.

Wu P., R. Wood, and P. Stott (2005), Human influence on increasing Arctic river discharges, *Geophys. Res. Lett.*, 32, L02703, doi:10.1029/2004GL021570.

Zhang, Y., J.M. Wallace, and D.S. Battisti (1997), ENSO-like interdecadal variability: 1900-93, *J. Clim.*, 10, 1004-1020.

List of figures

Figure 1. Location of the tide gauges included in this study (12 regions: cpacific- Central Pacific, neatlantic- Northeast Atlantic, nepacific- Northeast Pacific, nwatlantic- Northwest Atlantic, sepacific- Southeast Pacific, swatlantic- Southwest Atlantic, wpacific- Western Pacific, Antarctic- Antarctica, arctic- Arctic, baltic- Baltic, indian- Indian, mediterr- Mediterranean).

Figure 2. Comparison of the Northeastern Atlantic sea level rates from monthly data (top and zoomed inset showing generally close agreement in the two estimates) and associated

standard error (bottom) estimated using bi-weight robust means (black) and the virtual station method (grey) from Equation (1).

Figure 3. Normalized square rooted power spectrum of the mismatch error between each of the regions (Figure 1), except the Baltic, and the mean global sea level rate, calculated using an order 6 maximum entropy method. The thick black curve is the region mean spectrum. The power spectrum peaks at low frequencies due to long period oscillations, while the high frequency tail represents the “correct” mismatch error.

Figure 4. Rates of nonlinear sea level trends in the regions defined in Figure 1, found using an SSA embedding dimension equivalent to 30 years. Errors are not shown in the plot, but using the example of Figure 2 for Northeastern Atlantic, the maximum error at the start of the time series would be about $150P/\sqrt{(12 \times 30 \times 2)} = 2\text{-}3 \text{ mm yr}^{-1}$ and the minimum error about 1 mm yr^{-1} , other regions will have similar errors. Note that extrapolation at data boundaries means that curves are increasingly more uncertain within 30 years of the start and end of the records.

Figure 5. Top: Nonlinear trend (thick black line) in global sea level using an SSA embedding dimension equivalent to 30 years. Paralleling the trend is the 95% confidence interval in the trend found by considering the mismatch between the regional sea level curves, thin curve is the yearly global sea level. Bottom: the rate of the global sea level trend, and its standard error from Equation (4).

Figure 6. Rate of the nonlinear global sea level trend (thick black line, mm/yr) and stratospheric aerosol optical depth (thin line) [*Sato et al.*, 1993].

Figure 7. (a) Standardized sum of the statistically significant (at the 95% confidence level against red noise model) SSA components for the 3.5- and 2.4- year oscillations in time series of mean sea level in Northeastern Atlantic region; (b) for 5.2 – year oscillations in Northeastern Pacific. Both showing increased amplitude since 1950.

Figure 8. Wavelet power spectrum (Morlet) of mean monthly mean sea level for the Northeastern Atlantic (a); Northeastern Pacific (b); Mediterranean (c); Indian (d). Contours are in variance units. In all panels the black thick line is the 5 % significance level using the red noise model, solid line indicates the cone of influence. The colour bar represents normalized variances. All of the time series show an increase of power in the wavelet power spectrum at 2-30 year periods since 1940s as can be seen by the spread of the red and yellow shading to the upper rights of the panels.

Figure 9. The wavelet coherency between AO/sea level in the Northeastern Atlantic (a); b) the same for the NAO/Mediterranean sea level; c) the same for the SOI/Indian ocean sea level; d) the same for the SOI/Northeastern Pacific sea level. Contours are wavelet squared coherencies. The vectors indicate the phase difference (a horizontal arrow pointing from left to right signifies in-phase and an arrow pointing vertically upward means the second series lags the first by 90 degrees (i.e. the phase angle is 270°). In all panels the black thick line is the 5 % significance level using the red noise model. Data analyzed are annual sea level.

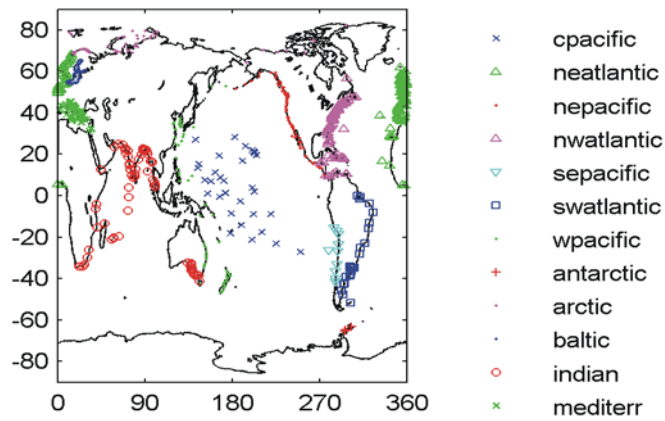


Figure 1. Location of the tide gauges included in this study (12 regions: cpacific- Central Pacific, neatlantic- Northeast Atlantic, nepacific- Northeast Pacific, nwatlantic- Northwest Atlantic, sepacific- Southeast Pacific, swatlantic- Southwest Atlantic, wpacific- Western Pacific, Antarctic- Antarctica, arctic- Arctic, baltic- Baltic, indian- Indian, mediterr- Mediterranean).

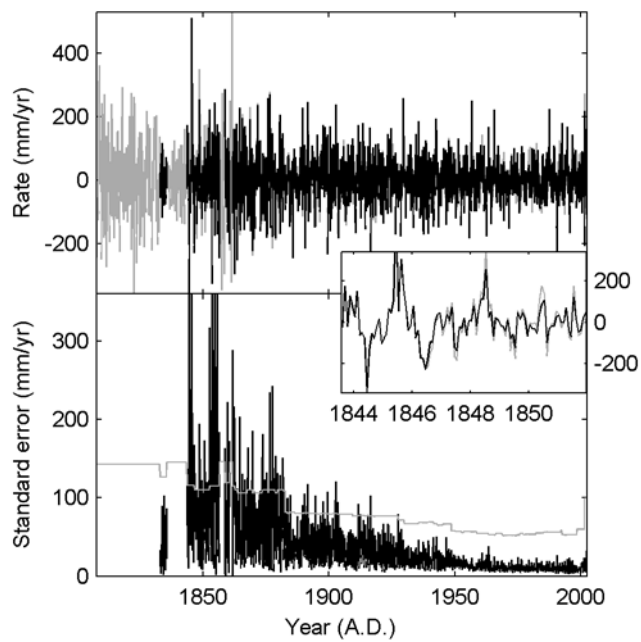


Figure 2. Comparison of the Northeastern Atlantic sea level rates from monthly data (top and zoomed inset showing generally close agreement in the two estimates) and associated standard error (bottom) estimated using bi-weight robust means (black) and the virtual station method (grey) from Equation (1).

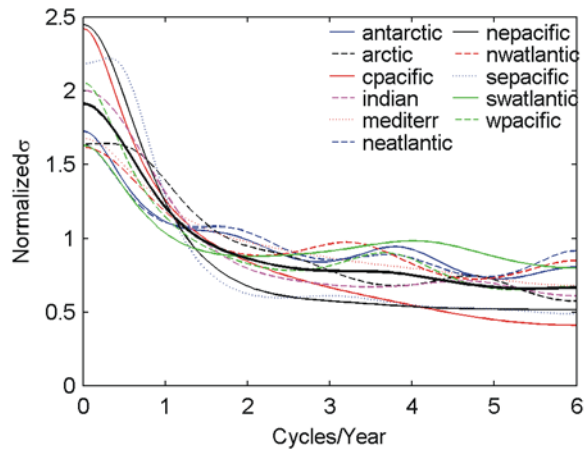


Figure 3. Normalized square rooted power spectrum of the mismatch error between each of the regions (Figure 1), except the Baltic, and the mean global sea level rate, calculated using an order 6 maximum entropy method. The thick black curve is the region mean spectrum. The power spectrum peaks at low frequencies due to long period oscillations, while the high frequency tail represents the “correct” mismatch error.

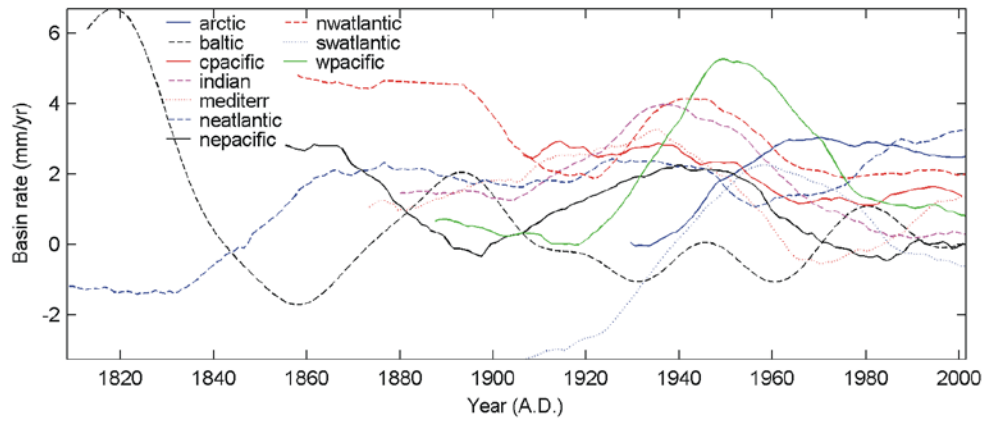


Figure 4. Rates of nonlinear sea level trends in the regions defined in Figure 1, found using an SSA embedding dimension equivalent to 30 years. Errors are not shown in the plot, but using the example of Figure 2 for Northeastern Atlantic, the maximum error at the start of the time series would be about $150P/\sqrt{(12 \times 30 \times 2)} = 2-3 \text{ mm yr}^{-1}$ and the minimum error about 1 mm yr^{-1} , other regions will have similar errors. Note that extrapolation at data boundaries means that curves are increasingly more uncertain within 30 years of the start and end of the records.

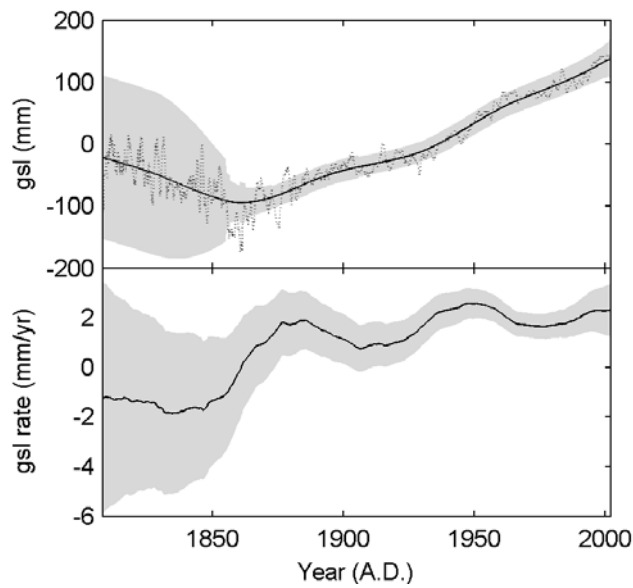


Figure 5. Top: Nonlinear trend in global sea level using an SSA embedding dimension equivalent to 30 years. Paralleling the trend is the 95% confidence interval in the trend found by considering the mismatch between the regional sea level curves, dashed curve is the yearly global sea level. Bottom: the rate of the global sea level trend, and its standard error from Equation (4).

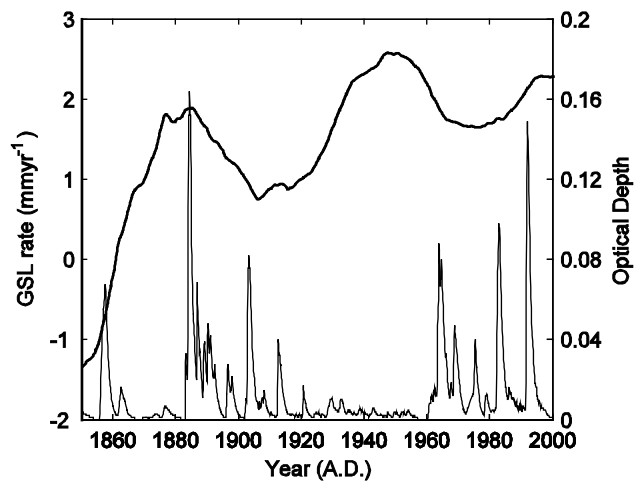
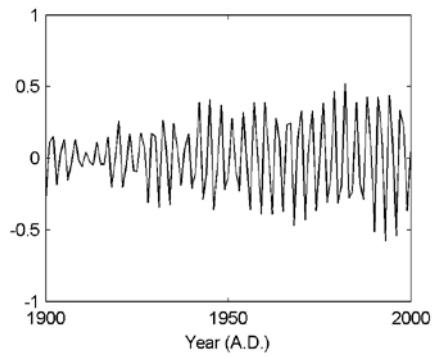
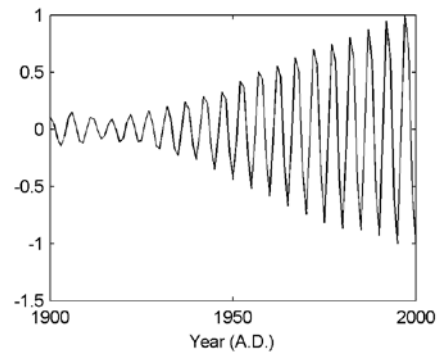


Figure 6. Rate of the nonlinear global sea level trend (thick black line, mm/yr) and stratospheric aerosol optical depth (thin line) [Sato *et al.*, 1993].

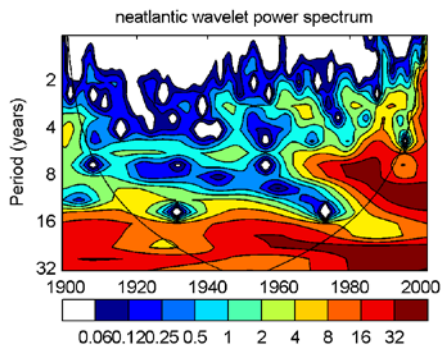


a

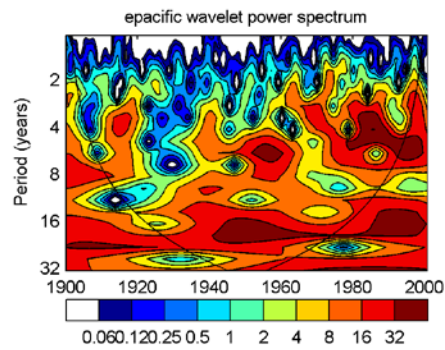


b

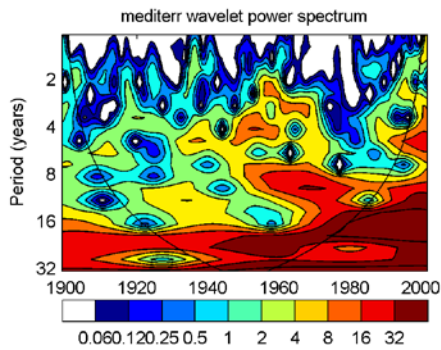
Figure 7. (a) Standardized sum of the statistically significant (at the 95% confidence level against red noise model) SSA components for the 3.5- and 2.4- year oscillations in time series of mean sea level in Northeastern Atlantic region; (b) for 5.2 – year oscillations in Northeastern Pacific. Both showing increased amplitude since 1950.



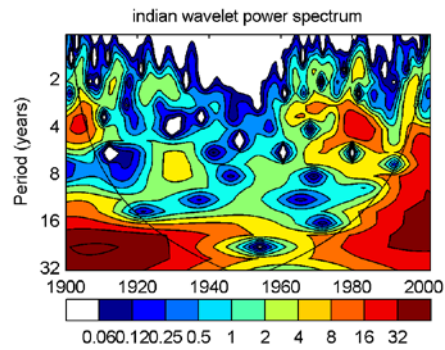
a



b



c



d

Figure 8. Wavelet power spectrum (Morlet) of mean monthly mean sea level for the Northeastern Atlantic (a); Northeastern Pacific (b); Mediterranean (c); Indian (d). Contours are in variance units. In all panels the black thick line is the 5 % significance level using the red noise model, solid line indicates the cone of influence. The colour bar represents normalized variances. All of the time series show an increase of power in the wavelet power spectrum at 2-30 year periods since 1940s as can be seen by the spread of the red and yellow shading to the upper rights of the panels.

Figure 7. (a) Standardized sum of the statistically significant (at the 95% confidence level against red noise model) SSA components for the 3.5- and 2.4- year oscillations in time series of mean sea level in Northeastern Atlantic region; (b) for 5.2 – year oscillations in Northeastern Pacific. Both showing increased amplitude since 1950.

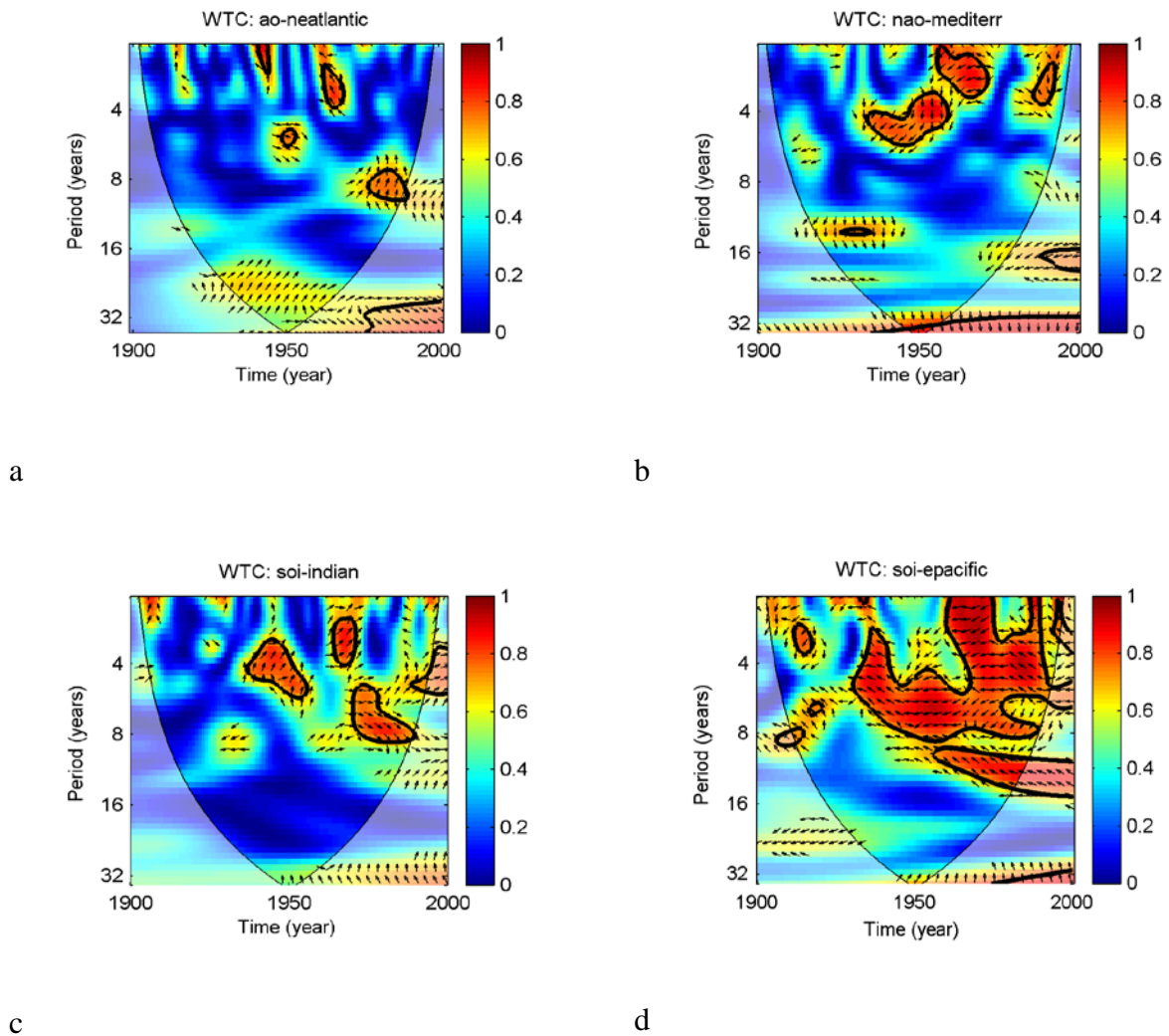


Figure 9. The wavelet coherency between AO/sea level in the Northeastern Atlantic (a); b) the same for the NAO/Mediterranean sea level; c) the same for the SOI/Indian ocean sea level; d) the same for the SOI/Northeastern Pacific sea level. Contours are wavelet squared coherencies. The vectors indicate the phase difference (a horizontal arrow pointing from left to right signifies in-phase and an arrow pointing vertically upward means the second series lags the first by 90 degrees (i.e. the phase angle is 270°). In all panels the black thick line is the 5 % significance level using the red noise model. Data analyzed are annual sea level.